A novel two-dimensional mercury antimony telluride: low temperature synthesis and characterization of RbHgSbTe₃

$$RbHgSbTe_3$$

Jing Li[a,*], Zhen Chen[a], Xunxie Wang[b], Davide M. Proserpio[c]

[a]*Department of Chemistry, Rutgers University, Camden, NJ 08102, USA*
[b]*Department of Physics, Rutgers University, Camden, NJ 08102, USA*
[c]*Dipartimento di Chimica Strutturale e Stereochimica Inorganica Universita' di Milano, 20133 Milano, Italy*

Abstract

RbHgSbTe₃ (I), a novel two-dimensional quaternary mercury antimony telluride, was synthesized via an unconventional low-temperature route. Single crystals of I were grown at 180°C from solvothermal reactions using ethylenediamine as solvent. The crystal structure of I was determined by X-ray diffraction methods. The structure belongs to the orthorhombic crystal system, space group $Cmcm$ (no. 63), a = 4.590 (2) Å, b = 15.745 (4) Å, c = 11.737 (2) Å, Z = 4. The crystal structure of this compound consists of two-dimensional layers of $_{\infty}^2[HgSbTe_3^-]$ with Rb⁺ counterions located between the layers. Optical studies performed on the powder samples of I suggested that the compound is a narrow-gap semiconductor. A band-gap of 0.2 eV was estimated from its diffuse reflectance spectrum. © 1997 Elsevier Science S.A.

Keywords: Mercury antimony telluride; Solvothermal reaction; Layered structure

1. Introduction

Many of the solid state materials with interesting chemical and physical properties were synthesized in the old fashioned way at relatively high temperatures (e.g. 500°C and above). The use of lower temperature routes to metastable phases have demonstrated that a number of compounds with unique structural features, unprecedented electronic, optical and catalytic properties can only be obtained under mild conditions. Our approaches to the low-temperature synthesis of solid state chalcogenides focus mainly on the exploration of solvothermal reactions below 200°C. By

incorporating chalcophilic elements into these reactions, we have produced a number of new compounds with extended one-, two- and three-dimensional structural frameworks and molecular tellurometalates containing elements such as mercury [1a,1b,1c], indium [2], tin [3], and silver [4]. Most of these are not obtainable by high temperature methods. While binary and ternary mercury and antimony chalcogenides have been studied quite extensively, the number of known quaternary phases is very limited. In fact, KHgSbS₃ is the only example whose crystal structure has been reported [5]. Here we report on the low-temperature solvothermal synthesis, crystal structure determination and optical studies of the first quaternary mercury antimony telluride, RbHgSbTe₃ (I).

*Corresponding author.

2. Experimental section

2.1. Chemicals

Mercury (I) chloride, (99.5%, Fisher Scientific), Te (99.8%, Aldrich Chemical Co.), Rb_2Te and Sb_2Te_3 were used as starting materials. Rb_2Te was prepared by direct combination of Rb and Te in liquid ammonia and Sb_2Te_3 was prepared by direct synthesis of Sb and Te in stoichiometric amounts. Ethylenediamine (99%, anhydrous, Fisher Scientific) was used as the solvent in all reactions.

2.2. Crystal growth of $RbHgSbTe_3$ (I)

Black needle crystals of I were grown initially in a reaction containing 0.075 g (0.25 mmol) of Rb_2Te, 0.059 g (0.125 mmol) of Hg_2Cl_2, 0.100 g (0.25 mmol) of Sb_2Te_3 and 0.096 g (0.75 mmol) of Te as starting materials. These starting materials were weighed and mixed in a glove box under an inert argon atmosphere. A thick-wall Pyrex tube (9 mm o.d., approx. 5 inches long) was used as the reaction vessel. Approximately 5.5 mmol of the solvent, ethylenediamine (en), was added to the mixture. The tube was then sealed under vacuum (approx. 10^{-3} torr) after the liquid was condensed by liquid nitrogen. The reaction took place in an oven at 180°C for 7 days. After cooling to room temperature, the reaction product was washed with 35% and 95% ethanol and dried with diethyl ether. Crystals of I were collected in a yield of approximately 15%. The remaining product was identified by powder X-ray diffraction to be Te (60%), Sb_2Te_3 (15%) and HgTe (10%). The approximate composition of I was obtained by microprobe analysis on the selected crystals using a JEOL JXA-8600 Superprobe.

2.3. Direct synthesis of powder samples

In the subsequent reactions, attempts were made to obtain a single phase of I. Direct syntheses by mixing stoichiometric amounts of Rb_2Te, Sb_2Te_3 (or Sb) and HgTe were made at different temperatures. Powder X-ray diffraction analysis showed that a high yield (> 85%) was produced in reactions conducted at 400°C using Rb_2Te, Sb_2Te_3 and HgTe in a 1:1:2 ratio. A small amount of Sb_2Te_3 was also found in the final product. As the temperature increased to 600°C, the yield decreased to approximately 60%. Reactions at 800°C produced almost exclusively HgTe with a small amount of Sb_2Te_3. Alternatively, using Rb_2Te, Sb, HgTe and Te as starting materials (1:2:2:3) resulted predominantly in unreacted Te and binary phases: approximately 90% HgTe and 10% Te at 400°C, 60% HgTe and 40% Te at 600°C and 40% Sb_2Te_3 and 60% Te at 800°C.

2.4. Single crystal structure determination

A black needle crystal (0.01 × 0.01 × 0.12 mm) of I was mounted on glass fiber in air on an Enraf-Nonius CAD4 automated diffractometer, and 25 intense reflections [17° < 2θ < 23°] were centered using graphite-monochromated Mo-Kα radiation (0.71069 Å). Least-squares refinement of their setting angles resulted in the unit-cell parameters reported in Table 1, together with other details associated with data collection and refinement. Data were collected using the ω-scan method with a scan interval of 1.5°, within the limits 6° < 2θ < 50° for −5 ≤ h < 5, 0 ≤ k ≤ 18, 0 ≤ l ≤ 13. The diffracted intensities were corrected for Lorentz and polarization effects. No decay was observed. An empirical absorption correction based on Ψ-scans was applied to all data (transmission range 1.0–0.57). The structure was solved by direct methods with SIR92 [6] and refined by full-matrix least-squares on F_o^2 using all the 447 independent reflections and 25 parameters (for 892 data collected). Anisotropic thermal displacements were assigned to all atoms. The final difference electron density map shows no features with a height greater than 6% of an Rb atom. All calculations were performed using SHELX-

Table 1
Crystallographic data for $RbHgSbTe_3$ (I)

Chemical formula	$RbHgSbTe_3$	Formula weight	790.61
Crystal system	Orthorhombic	Space group	*Cmcm* (no. 63)
a =	4.590(2) Å	T =	20°C
b =	15.745(4) Å	V =	848.2(5) Å³
c =	11.737(2) Å	ρ_{calc} =	6.191 g cm³
Z =	4	μ =	36.971 mm⁻¹
R indices[a] $[F_o > 4\sigma(F_o)]$ (298 data)		R1 0.0450, wR2 0.0738	
R indices[b] (all data)		R1 0.0889, wR2 0.0861	

[a] $R1 = \Sigma||F_o| - |F_c||/\Sigma|F_o|$.
[b] $wR2 = [\Sigma(F_o^2 - F_c^2)^2/\Sigma wF_o^4]^{1/2}$.
Weighting: $w = 1/[\sigma^2(F_o^2) + (0.0255P)^2]$ where $P = (F_o^2 + 2F_c^2)/3$.

93 [7]. The unique Sb atoms lie 0.47 Å from the origin (2/m) on a Wyckoff position 8f. This produces an unrealistic very short Sb–Sb contact of 0.94 Å. Imposing half occupancy on the Sb site obtains the correct expected formula, RbHgSbTe$_3$ in agreement with the formal charges Rb($+1$), Hg($+2$), Sb($+3$) and Te(-2) and the microprobe analysis. Crystal drawings were produced with SCHAKAL [8]. Final atomic coordinates, average temperature factors, selected bond lengths and angles are reported in Tables 2 and 3.

2.5. Diffuse reflectance measurements

To investigate the band-gap energy and the band structure of I, experiments were conducted to measure its optical diffuse reflectance spectra at room temperature using a Shimadzu UV-3101PC double beam, double monochromator spectrophotometer. The wavelength of the radiation beam was in the range 200–3200 nm. Initially, the 100% line flatness of the spectrophotometer was set by using barium

Table 2
Atomic coordinates and equivalent isotropic displacement parameters (Å^2) for RbHgSbTe$_3$ (I). U (eq) is defined as one-third of the trace of the orthogonalized Uij tensor

Atom	x	y	z	U (eq)
Hg	0	0.45160(12)	1/4	0.0265(5)
Rb	1/2	0.2475(3)	1/4	0.0348(10)
Te (1)	1/2	0.5643(2)	1/4	0.0234(7)
Te (2)	0	0.36316(12)	0.0440(2)	0.0281(6)
Sb^a	1/2	0.5297(2)	0.4948(3)	0.0225(10)

^{a} s.o.f. 0.5.

Table 3
Selected bond lengths (Å) and angles (degree) for RbHgSbTe$_3$

Hg–Te(1)	2 × 2.790(2)	Hg–Te(2)	2 × 2.991(2)
Sb–Te(1)	2.925(4)	Sb–Te(2)	2 × 2.906(3)
Sb···Te(1)	3.341(4)	Sb···Te(2)	2 × 3.514(3)
Rb···Te(1)	2 × 3.685(4)	Rb···Te(2)	4 × 3.799(3), 2 × 3.866(3)
Te(1)–Hg–Te(2)	4 × 107.78(3)	Te(2)–Hg–Te(2)	102.12(10)
Te(1)–Hg–Te(1)	104.56(10)	—	—
Te(1)–Sb–Te(2)	2 × 94.99(9)	Te(2)–Sb–Te(2)	104.32(13)

sulfate (BaSO$_4$). A powder sample of RbHgSbTe$_3$ was mounted on the sample holder housed on an ISR-3100 UV-VIS-NIR Integrating Sphere attachment. To ensure the maximum reflection an approximately 1.0–2.0 mm thick BaSO$_4$ layer was placed underneath the sample. The diffuse reflectance data of the sample were taken by a computerized data acquisition program (UVPC v.3.7, Shimadzu).

The thickness of the sample was approximately 2.0–3.0 mm, which was much greater than the size of the individual particles. Therefore, an ideal diffuse reflection can be assumed, and the scattering factor (S) can be taken as a constant. The absorption coefficient (α) can be computed using the Kubelka–Munk or remission function [9]:

$$\alpha = \text{const.}(1 - R_\infty)^2/2R_\infty$$

Experimental results for the absorption coefficients for I are shown in Fig. 1, in which the F-function (α/S) is plotted against photon energy ($h\nu$). By fitting
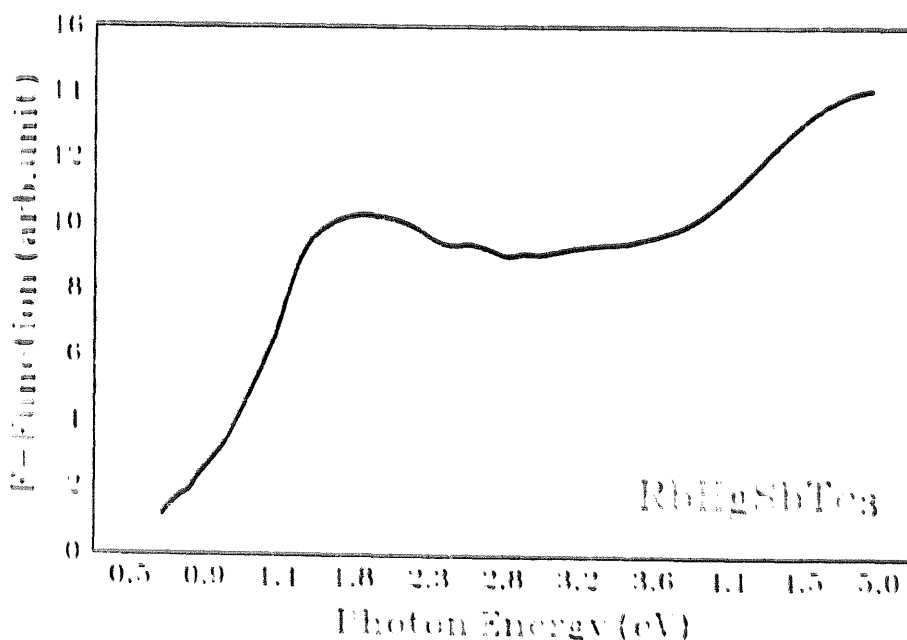

Fig. 1. Optical absorption spectrum and empirical fit for RbHgSbTe$_3$ (I). The empirical fit gives $\alpha = \text{const.}(h\nu - 0.183)^2$, indicating an indirect transition process.
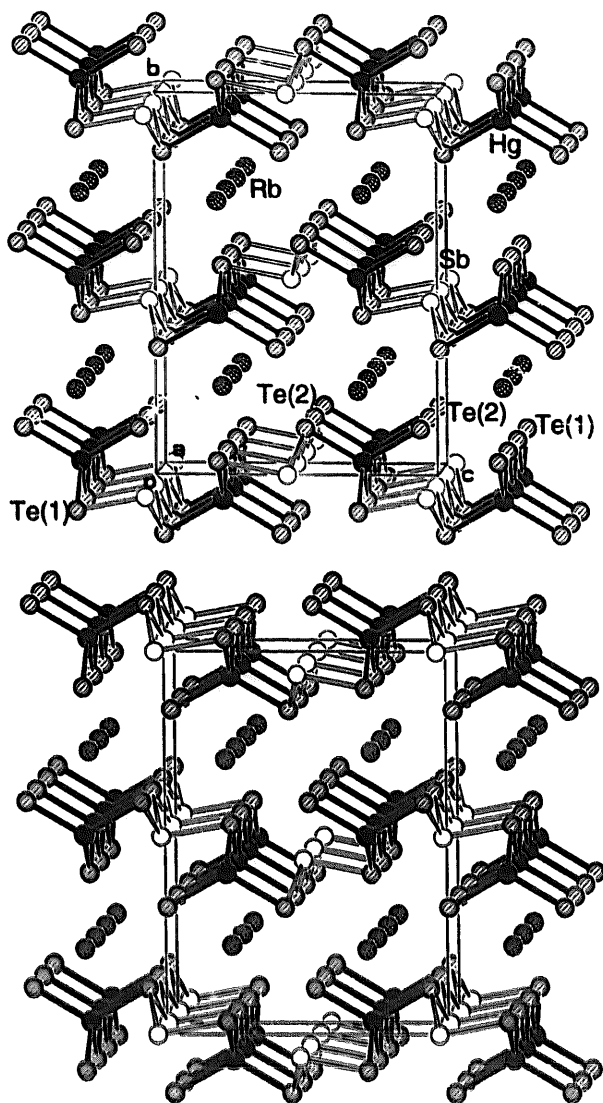
Fig. 2. Unit cell contents of two possible ordered structures of RbHgSbTe₃.

the sharp edge of α/S vs. photon energy, $h\nu$, and extrapolating the fitting curve to photon energy axis, the value of the gap energy (or more precisely, the optical band-gap energy), $E_G = 0.183$ eV, was determined. The best empirical fitting of the absorption was found to be $\alpha = \text{const.}(h\nu - 0.183)^2$.

3. Results and discussion

RbHgSbTe₃ represents a new layered structure type with Rb⁺ cations located between the layers. As shown in Fig. 2, it consists of $^2_\infty[\text{HgSbTe}_3^-]$ two dimensional networks, formally generated by linking chains of corner sharing tetrahedra $^1_\infty[\text{HgTe}_3^{4-}]$ with Sb³⁺ atoms. The assignment of Sb and Te atoms was based on their chemically reasonable connectivity and microprobe analysis whose average was 1.0:1.1:1.0:3.1. To have symmetrical coordination around the chains, antimony occupies one of the two possible sites (vide

supra) in such a way as to give two types of equivalent ordered layers that pack for example as in the two $Cmc2_1$ structures (acentric subgroup of $Cmcm$) shown in Fig. 2. The presence of Sb in one of the two possible positions in one layer is uncorrelated with the layers above or below. Energetically the two types of layers are equivalent, giving as a final result the $Cmcm$ symmetry observed. A top view of one layer is shown in Fig. 3. The Hg forms a distorted tetrahedron with the Te (Te–Hg–Te ave. 106(2)° and Hg–Te ave. 2.85(6) Å), with distances comparable with tetracoordinated Hg found in Rb₂Hg₃Te₄ [1c], (Hg₄Te₁₂)⁴⁻ [10a], $^1_\infty[\text{Hg}_3\text{Te}_7^{4-}]$ [10b], and (HgTe₈)²⁻ [10c] (2.69–2.97 Å). The distorted octa-coordination of Sb with three short and three long contacts (shown in Fig. 4) is similar to the one observed in the A₃SbTe₃ (A = K [11a,11b], Na [11c] and isostructural K₃BiTe₃ [11d]) with isolated (SbTe₃)³⁻ pyramids and in BaSbTe₃ [12a] (see also the isostructural BaBiTe₃ [12b]). The short Sb–Te bond distances in I are within the range (2.77–3.09 Å) observed in compounds containing Sb–Te (bridging) bonds such as BaSbTe₃ [12a] and in several Zintl anions reported by Haushalter et al.: (Sb₉Te₆)³⁻ [12a,12b], (Cu₄SbTe₁₂)³⁻ [13a,13b,13d], (Sb₂Te₅)⁴⁻ [13a,13c,13d], (Sb₆Te₉)⁴⁻ [13a,13c,13d], (SbTe₄)³⁻ [13a,13e]. The eight long Rb⋯Rb contacts define a bicapped trigonal prism as illustrated in Fig. 4, with the two longest contacts (3.866(3) Å) defining the capping Te(2) atoms. The shortest interlayer Te(2)⋯Te(2) contact of 4.363(3) Å is longer than the sum of van der Waals radii of 4.12 Å, which eliminates any significant Te–Te bonding between the layers. Formal oxidation state assignment suggests that I is electron precise and is most likely a semiconductor.

RbHgSbTe₃ is the first quaternary mercury antimony telluride and one of the few mercury tellurides containing a two-dimensional network. As far as we are aware, the only other known example is Rb₂Hg₃Te₄ [1c]. A chemically related compound is KHgSbS₃ [5], which is the only other known quaternary mercury antimony chalcogenide. KHgSbS₃ has a one-dimensional structure that contains pyramidal (SbS₃)3⁻ and almost linear coordination of Hg [5].

Optical absorption spectra have been extensively used as one of the most important tools for probing the energy gaps and band structures of semiconductors [14–16]. Due to the quantized band structure of a semiconductor, the absorption spectrum is strongly dependent on the energy of the quanta of the incident electromagnetic wave. In principle, the absorption spectrum of a semiconductor displays a sharp increase (absorption edge) when a photon energy, $h\nu$, is equal to the gap energy, E_G. Such behavior results fundamentally from the creation of electron-hole pairs and
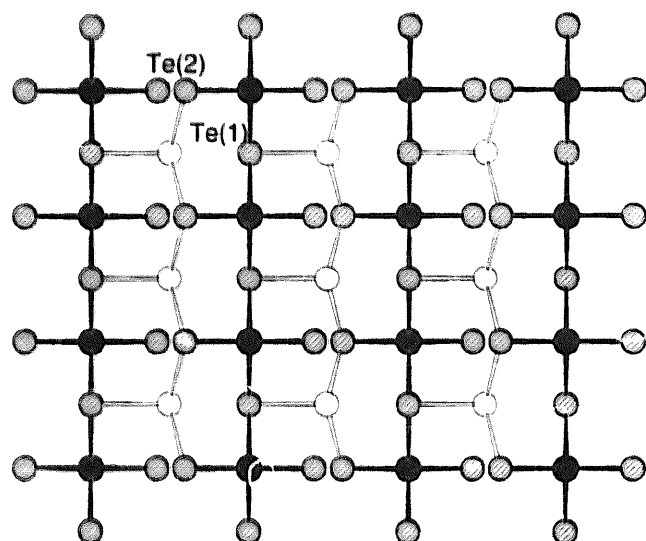
Fig. 3. View down b axis of one layer of ²[HgSbTe₃].

Fig. 4. Coordination of the antimony (top) and coordination of the Rb cation (bottom).

transport of electrons from valance band to conduction band [17]. The threshold of continuous optical absorption (absorption edge) can be explained by the quantum mechanical perturbation theory of electron–photon interaction [18]. For different transition mechanisms, it has been proved that along the sharp absorption edge, the energy of incident photons and the energy of the band-gap of the semiconductor have a simple relation as [18,19]:

$$\alpha = const.(h\nu - E_G)^n$$

or

$$\alpha = const.(h\nu - E_G)^n/h\nu$$

where the index n depends on the interband transition mechanism. If $n = 1/2$, the interband transition is the allowed direct transition; for $n = 3/2$, the transition is the forbidden direct transition; and for $n = 2$ the transition is an indirect one [20]. Experimentally, the expressions have been successfully applied to explain the absorption edges of a number of semiconductors [16–19,21–23].

It is of interest to point out that the fitting index parameter for RbHgSbTe₃ (I) is 2, which indicates that the interband transition in this material is of the indirect transition. In such a case, an additional phonon must be absorbed or emitted so as to keep the total momentum conserved in the electron–photon interaction process [18]. It is apparent that there are several small shoulders along the absorption edge in the spectrum, which is typical for an indirect transition. Those staircase-like shoulders indicate the threshold for the formation of free excitons with emission or absorption of phonons. Similar structures were observed in Ge, Si, and GaP materials, etc. [24].
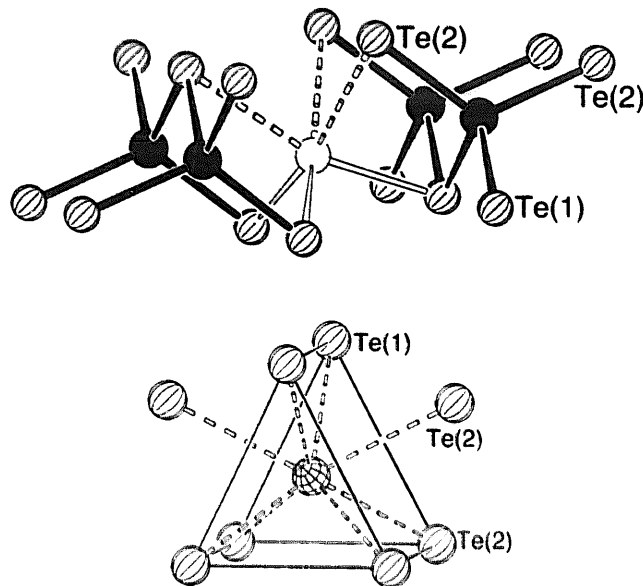
In addition, since the absorption spectrum was measured at room temperature, the phonon energy involved in the indirect interband transition is rather small compared to the band-gap energy and thus can be neglected [17,21]. Assuming this is true for the absorption edge of RbHgSbTe₃ measured at room temperature, we might conclude that this material is a narrow-gap semiconductor with an assessed small (optical) band-gap energy of 0.2 (0.183) eV. The small band-gap of I is consistent with its black color. In fact, narrow band gaps have been observed in a number of other Sb-containing materials, for example, PtSb (0. 1 eV), Sb₂Te₃ (0.2 eV), InSb (0.2 eV), CdSb (0.5 eV), ZnSb (0.5 eV) and GaSb (0.7 eV) [19,21].

Acknowledgements

References

[1a] J. Li, B.G. Rafferty, S. Mulley, D.M. Proserpio, Inorg. Chem. 34 (1995) 6417.

[1b] J. Li, Z. Chen, J.L. Kelley, D.M. Proserpio, Mater. Res. Soc. Symp. Proc., 453 (1997) (in press).

[1c] J. Li, Z. Chen, K.-C. Lam, S. Mulley, D.M. Proserpio, Inorg. Chem. 36 (1997) 684.

[2] J. Li, Z. Chen, T.J. Emge, D.M. Proserpio, Inorg. Chem., 36 (1997) 1437. Z. Chen, J. Li, F. Chen, D.M. Proserpio, Inorg. Chim. Acta (submitted).

[3] J. Li, Z. Chen, T.J. Emge, T. Yuen, D.M. Proserpio, Inorg. Chim. Acta (submitted).

[4] J. Li, Z. Chen, D.M. Proserpio, Manuscript in preparation.

[5] M. Imafuku, I. Nakai, K. Nagashima, Mater. Res. Bull. 21 (1986) 493.

[6] A. Altomare, G. Cascarano, C. Giacovazzo, et al., ARTICLE TITEL. J. Appl. Crystallogr. 27 (1994) 435.

[7] G.M. Sheldrick, SHELX-93: Program for Structure Refinement, University of Goettingen, Germany, 1994.

[8] E. Keller, SCHAKAL 92: A Computer Program for the Graphical Representation of Crystallographic Models, University of Freiburg, Germany, 1992.

[9] W.M. Wesley, Wendlandt, G.H. Harry, Reflectance Spectroscopy, Interscience Publishers, John Wiley, New York/London/Sydney, 1966.

[10a] R.C. Haushalter, R.C. Angew, Chem. Int. Ed. Engl. 24 (1985) 433.

[10b] S.S. Dhingra, C.J. Warren, R.C. Haushalter, A.B. Bocarsly, Chem. Mater. 6 (1994) 2382.

[10c] M.G. Kanatzidis, Comments Inorg. Chem., 10 (1990) 161; J.C. Bollinger, L.C. Roof, D.M. Smith, J.M. McConnachie, J.A. Ibers, Inorg. Chem., 34 (1995) 1430.

[11a] J.-S. Jung, B. Wu, E.D. Stevens, C.J. O'Connor, J. Solid State Chem. 94 (1991) 362.

[11b] B. Eisenmann, R. Zagler, Z. Kristllogr. 197 (1991) 255.

[11c] B. Eisenmann, R. Zagler, Z. Kristllogr. 197 (1991) 257.

[11d] J. Lin, G.J. Miller, J. Solid State Chem. 113 (1994) 296.

[12a] K. Volk, G. Cordier, G. Cook, H.Z. Schafer, ARTICLE TITEL. Z. Naturforsch. 35B (1980) 136.

[12b] D.Y. Chung, S. Jobic, T. Hogan, et al., J. Am. Chem. Soc. 119 (1997) 2505.

[13a] C.J. Warren, D.M. Ho, R.C. Haushalter, A.B. Bocarsly, Agnew. Chem. Int. Ed. Engl. 32 (1993) 1646.

[13b] S.S. Dhingra, R.C. Haushalter, J. Am. Chem. Soc. 116 (1994) 3651.

[13c] C.J. Warren, S.S. Dhingra, D.M. Ho, R.C. Haushalter, A.B. Bocarsly, Inorg. Chem. 33 (1994) 2709.

[13d] C.J. Warren, R.C. Haushalter, A.B. Bocarsly, J. Alloys Comp. 229 (1995) 175.

[13e] J.L. Shreeve-Keyer, R.C. Haushalter, Polyhedron 15 (1996) 1213.

[14] S.M. Johnson, S. Sen, W.H. Konkel, M.H. Kalisher, J. Vac. Sci. Technol. B9 (1991) 1897.

[15] M. Ashraf Chaudhry, Anwar Manzoor Rana, M. Altaf, M. Shakeel Bila', Aust. J. Phys. 48 (1995) 887.

[16] Hartmut. Haug, Optical Nonlinearities and Instabilities in Semiconductors, Academic Press, Boston/San Diego/New York, 1988.

[17] O. Madelung, Introduction to Solid-State Theory, Springer-Verlage, Berlin, Heidelberg, New York, 1987.

[18] K. Seeger, Semiconductor Physics — an Introduction, 3rd ed., Springer-Verlag, Berlin-Heidelberg-New York-Tokyo, 1985

[19] N.F. Mott, E.A. Davis, Electronic Processes in Non-Crystalline Materials, 2nd ed., Oxford University Press, 1979.

[20] H.F. Wolf, Semiconductors, Wiley-Interscience, New York, London, Sydney, Toronto, 1971.

[21] J.I. Pankove, Optical Processes in Semiconductors, Prentice-Hall, Englewood Cliffs, New Jersey, 1971.

[22] S.P. Tandon, J.P. Gupta, Phys. Stat. Sol. 88 (1970) 363.

[23] T.J. McCarthy, S.-P. Ngeyi, J.-H. Liao, D.C. DeGroot, T. Hogan, C.R. Kannewurf, M.G. Kanatzidis, Chem. Mater., 5 (1993) 331; J.-H. Liao, M.G. Kanatzidis, Chem. Mater., 5 (1993) 1561; J.-H. Liao, C. Varotsis, M.G. Kanatzidis, Inorg. Chem., 32 (1993) 2453; T.J. McCarthy, M.G. Kanatzidis, Inorg. Chem., 34 (1995) 1257; K. Chondroudis, T.J. McCarthy, M.G. Kanatzidis, Inorg. Chem., 35 (1996) 840.

[24] C.F. Freeman, J. Vac. Sci. Technol. B9 (1991) 1613.